An efficient catalytic method for the synthesis of pyrido[2,3-*d*]pyrimidines as biologically drug candidates by using novel magnetic nano particles as a reusable catalyst

Saeid Moradi,[a] Mohammad Ali Zolfigol,*[a] Mahmoud Zarei,[a] Aria Tajally,[a] Diego A. Alonso,*[b] Abbas Khoshnood*[b]

[a]Depatment of Organic Chemistry, Faculty of Chemistry, Bu-Ali Sina University, Hamedan 6517838683, Tel: +988138282807, Fax: +988138380709 Iran. E-Mail: zolfi@basu.ac.ir & mzolfigol@yahoo.com.

[b]Organic Synthesis Institute and Organic Chemistry Department, Alicante University, Apdo. 99, 03080 Alicante, Spain. E-Mail: diego.alonso@ua.es, abbas.khoshnood@ua.es

Abstract: A convenient method for the synthesis of pyrido[2,3-*d*]pyrimidines by using the novel nanomagnetic silica-bonded *S*-sulfonic acid [Fe_3O_4@SiO_2@$(CH_2)_3$S-SO_3H] as an efficient and recyclable catalyst under solvent free condition is described. The major advantages of the present methodology are high yield, short reaction time, and reusability of the catalyst. Furthermore, the nanomagnetic silica-bonded *S*-sulfonic acid was fully characterized by using various techniques such as FT-IR, TG/DTG, DTA, EDX, μXRF, μXRF elemental mapping, XRD, HRTEM, SEM, XPS, and N_2 physisorption. The results obtained from this research support the idea of rational designs, syntheses, and applications of tasked-specific and reusable catalysts for the synthesis of various polynitrogenated heterocyclic compounds containing 1,4-dihydropyridine moieties.

Keywords: Tasked-specific catalyst, Reusable catalyst, Nano magnetic silica-bonded *S*-sulfonic acid, Solvent free conditions, Pyrido[2,3-*d*]pyrimidines, Nitrogen heterocyclic compounds, 1,4-Dihydropyridines**.**

Introduction

Nowadays, the design of safer chemicals and chemical processes is of great interest.[1] In this sense, catalytic processes play a major role in environmental protection by reducing toxic waste and reaction times while keeping high yield conditions. Solid acids are known as important catalysts in a wide range of reactions because of their high activity and recyclability.[2] Among them, magnetic nano-catalysts are even more attractive due to their easy and fast separation from reaction media.

Nitrogenated heterocyclic compounds are invaluable candidates for the design and discovery of new biologically active compounds. Well-known examples are those molecules with 1,4-dihydropyridine (1,4-DHP) moieties which are considered as 'distinguished scaffolds' due to their bio- and pharmaceutical activities. Among them, 1,4-dihydropyridine derivatives are calcium channel blockers, cardiovascular agents for the treatment of hypertension,[3] antivirals,[4] antioxidants,[5] and anti-tumorals.[6,7] Therefore, 1,4-DHPs are good candidates for drug components, having been their syntheses and applications extensively reviewed.[8] Another remarkable feature of 1,4-DHPs as Hantzsch esters is their use as NAD(P)H (I) analogues (Figure 1) for the catalytic hydrogenation of unactivated aldehydes [9,10] and 1,2,4-triazolinediones.[11]

Regarding synthetic methodologies towards 1,4-dihydropyridines, Li *et al.* have recently synthesized pyrido[2,3-*d*]pyrimidines via a one-pot three component reaction of aromatic aldehydes, malononitrile, and 2,6-diaminopyrimidin-4-one using [bmim]BF_4 as solvent at 80 ^oC.[12] To the best of our knowledge, this is the only methodology towards pyrido[2,3-*d*]pyrimidines reported so far. Thus, the development of new and simple organic synthetic methods for the efficient preparation of this type of heterocycles is an interesting challenge in this field.

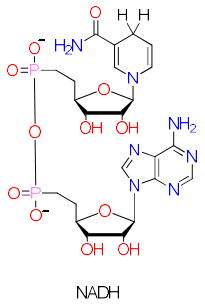

Figure 1: The molecular structure of NADH

Niknam *et al.* have reported the synthesis and application of a bulky, amorphous silica-bonded *S*-sulfonic acid (SBSSA) as a reusable catalyst for the preparation of aromatic 1,1-diacetates,[13] quinoxalines,[14] 4,4'-(arylmethylene) bis (1*H*-pyrazol-5-ols),[15] *α*-amino nitriles,[16] 1,8-dioxo-decahydroacridines, 1,8-dioxo-octahydroxanthenes,[17] bis (indolyl) methanes,[18] silylated alcohols,[19] trisubstituted dimidazoles,[20] 2,3-dihydroquinazolin-4(1*H*)-ones[21], and 2-aryl-1-arylmethyl-1*H*-1,3-benzimidazoles.[22]

A proper design, synthesis, and application of a given catalyst must consider important aims, such as recyclability, reusability, and proper tasked-specific behavior. Herein, following our recent interest on the rational design and synthesis of dihydropyridine derivatives for the development of new biomimetic reactions,[23] we wish to report an operative and one-pot synthetic method for the preparation of pyrido[2, 3-*d*]pyrimidines using novel magnetic nano particles of [Fe_3O_4@SiO_2@$(CH_2)_3$S-SO_3H] as a recyclable and reusable catalyst under neat conditions (Schemes 1 and 2).

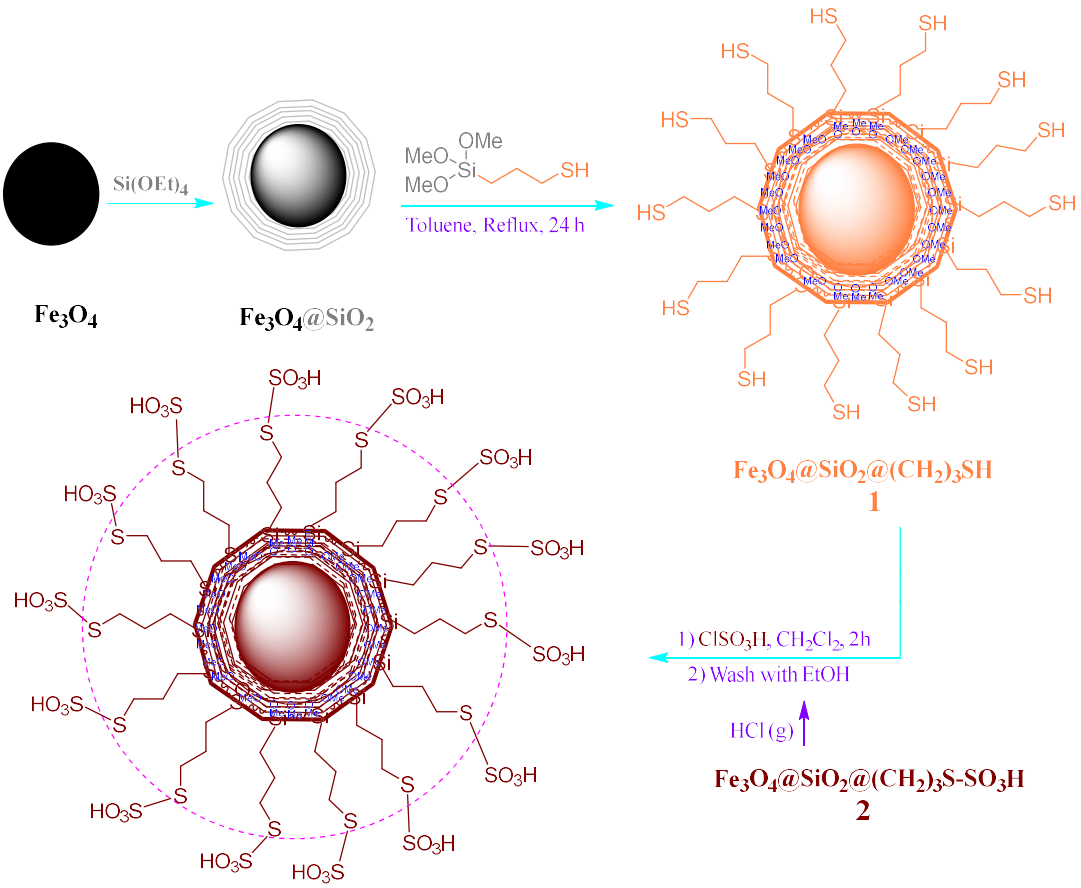

Scheme 1. Synthesis of magnetic nano catalyst [Fe_3O_4@SiO_2@$(CH_2)_3$S-SO_3H]

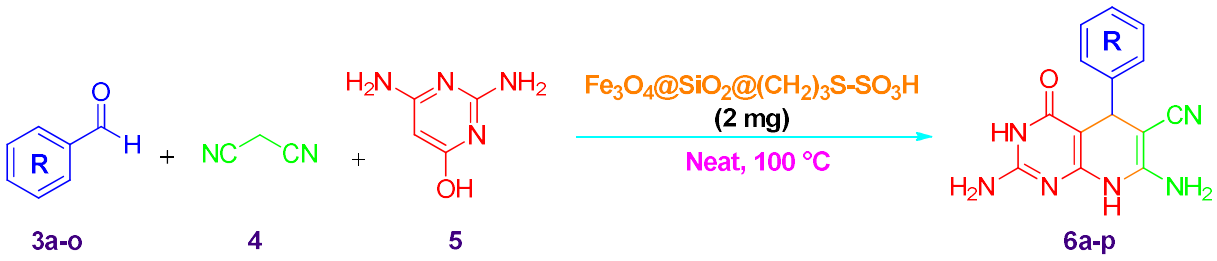

Scheme2. Synthesis of pyrido[2,3-*d*]pyrimidines **6a-p** promoted by magnetic nanocatalyst **2**.

Results and discussion

Fe_3O_4@SiO_2 nanoparticles and [Fe_3O_4@SiO_2@$(CH_2)_3$S-SO_3H] were synthesized following the procedure previously reported by our research group (Scheme 1).[24a] To ensure construction of the recoverable magnetic nanoporous catalyst **2**, this material was analyzed using different techniques

such as, Fourier transforms infrared spectroscopy (FT-IR), thermal gravimetric (TGA), derivative thermal gravimetric (DTG), differential thermal analysis (DTA), energy-dispersive X-ray spectroscopy (EDX), micro X-ray fluorescence (μXRF), μXRF elemental mapping, X-ray diffraction patterns (XRD), high resolution transmission electron microscopy (HRTEM), scanning electron microscopy (SEM), N_2 physisorption, and X-ray photoelectron spectroscopy (XPS) (Figures 2-9).

The FT-IR spectrum of the synthesize [Fe_3O_4@SiO_2@$(CH_2)_3$S-SO_3H] nano catalyst **2** was investigated and compared with the precursor material [Fe_3O_4@SiO_2@$(CH_2)_3SH$] **1** (Figure 2). As shown, both materials showed the corresponding Si-Si stretching absorption bands at 1077 and 1104 cm^{-1}, respectively. In the case of **2**, the broad absorption band at 1077 overlapped the symmetric stretching absorption band from the SO_2 moiety.

On the other hand, catalyst **2** also showed two more absorption bands at 649 and 1206 cm^{-1}, corresponding to the stretching vibration of the S-O bond and the asymmetric stretching vibration of the SO_2 group (Figure 2b).

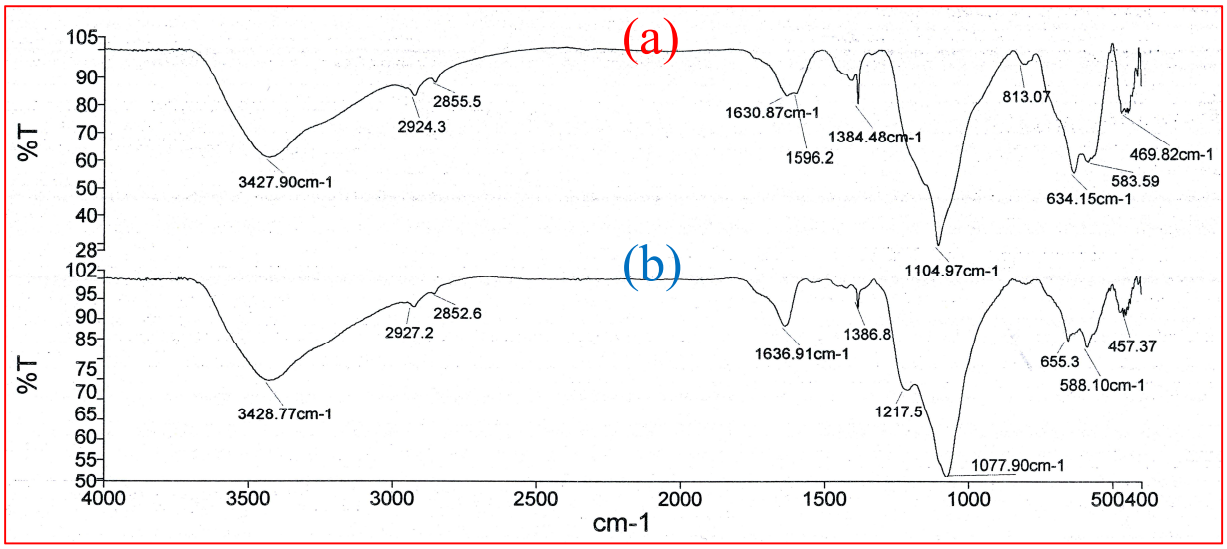

Fig. 2. FT-IR spectrum of two final steps a) Fe_3O_4@SiO_2@$(CH_2)_3SH$] and b) [Fe_3O_4@SiO_2@$(CH_2)_3$S-SO_3H]

In order to monitor the thermal stability and behavior of [Fe_3O_4@SiO_2@$(CH_2)_3$S-SO_3H], the thermogravimetry (TG), derivative thermogravimetry (DTG), and the differential thermal analysis (DTA) were conducted being the attained data depicted in Figures 3 and 4. Regarding TGA, the first weight loss step, related to the removal of surface-adsorbed water and organic solvents, took place between 25 and 105 °C and involved a weight loss of 4 wt%. Finally, the second and main weight loss region for [Fe_3O_4@SiO_2@$(CH_2)_3$S-SO_3H] (between 105 to 700 °C) could be ascribed to the continuing decomposition of the sulfur moieties of the catalyst. The weight loss for this step was calculated to be 28.7% which was clearly correlated with μXRF results (see Figure 5). The remaining 71.3 wt% of catalyst was attributed to the Fe_3O_4@SiO_2. Moreover, the DTA analysis diagram showed a general negative downward slope between 25 °C to 700 °C in which, decomposition of catalyst and its precursor in nitrogen atmosphere were exothermic (Figure 4).

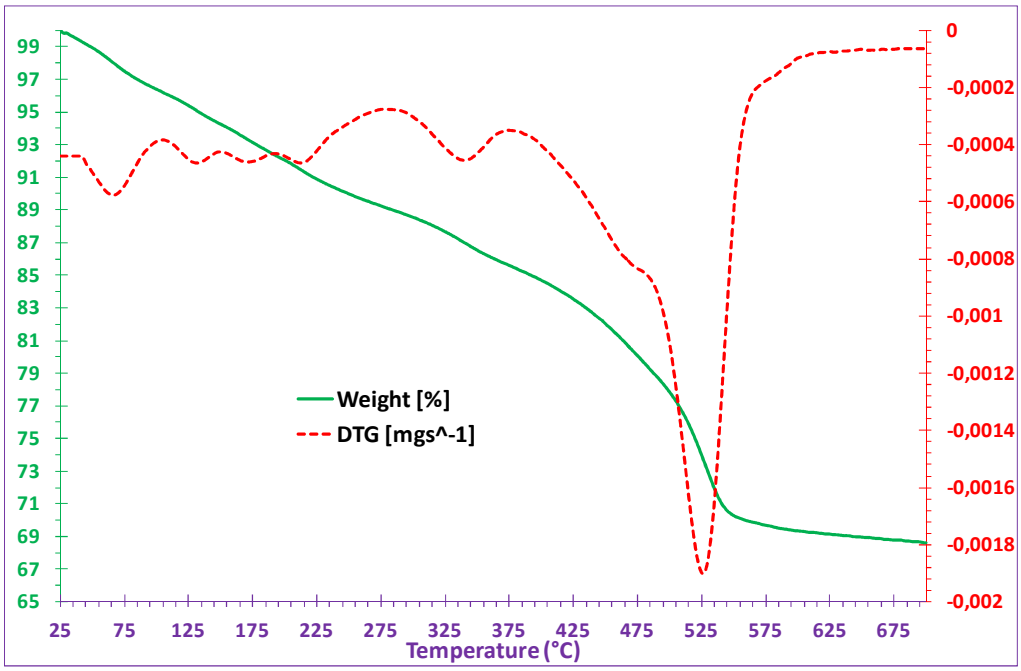

Fig. 3. Thermal gravimetric analysis (TG/DTG) analysis of nano [Fe_3O_4@SiO_2@$(CH_2)_3$S-SO_3H]

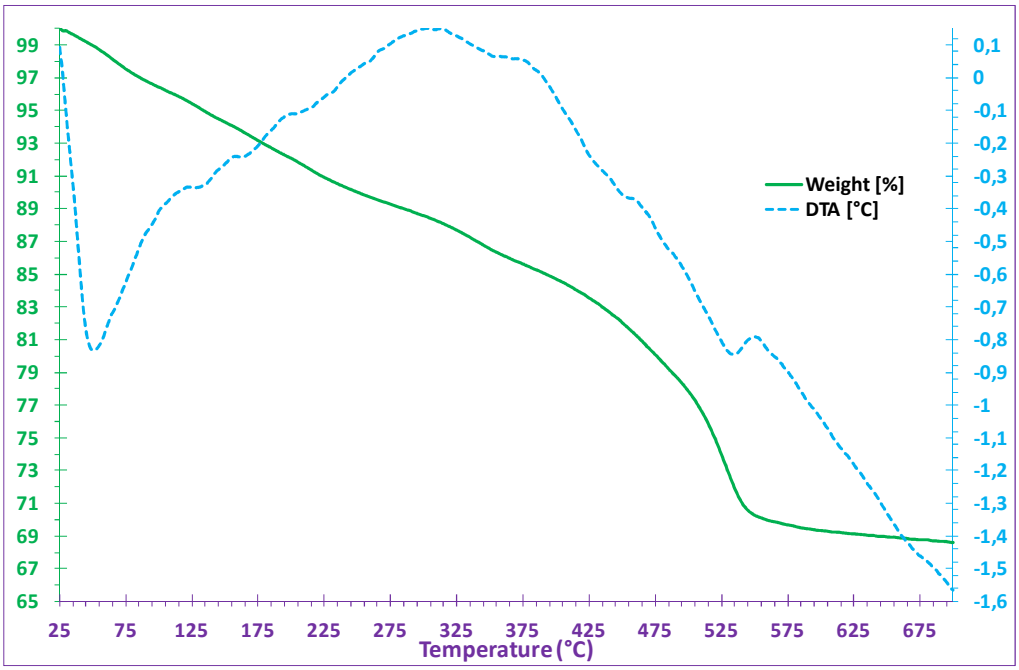

Fig. 4. Differential thermal analysis (TG/DTA) of nano [Fe_3O_4@SiO_2@$(CH_2)_3$S-SO_3H]

Next, micro X-ray fluorescence (μXRF), μXRF elemental mapping and energy-dispersive X-ray spectroscopy (EDX) analyses were used to determine the organic content and also the elemental composition of the nano-catalyst **2** (Figures 5a-f). As shown in Figure 5, the EDX and μXRF of **2** confirmed the presence of the expected elements in the catalyst structure, with a 29.44 wt% of sulfur content. Examination of the μXRF mapping images (Figures 5c-f) proved the presence of Si, Fe, and S elements in the catalyst with a good distribution over the catalyst surface.

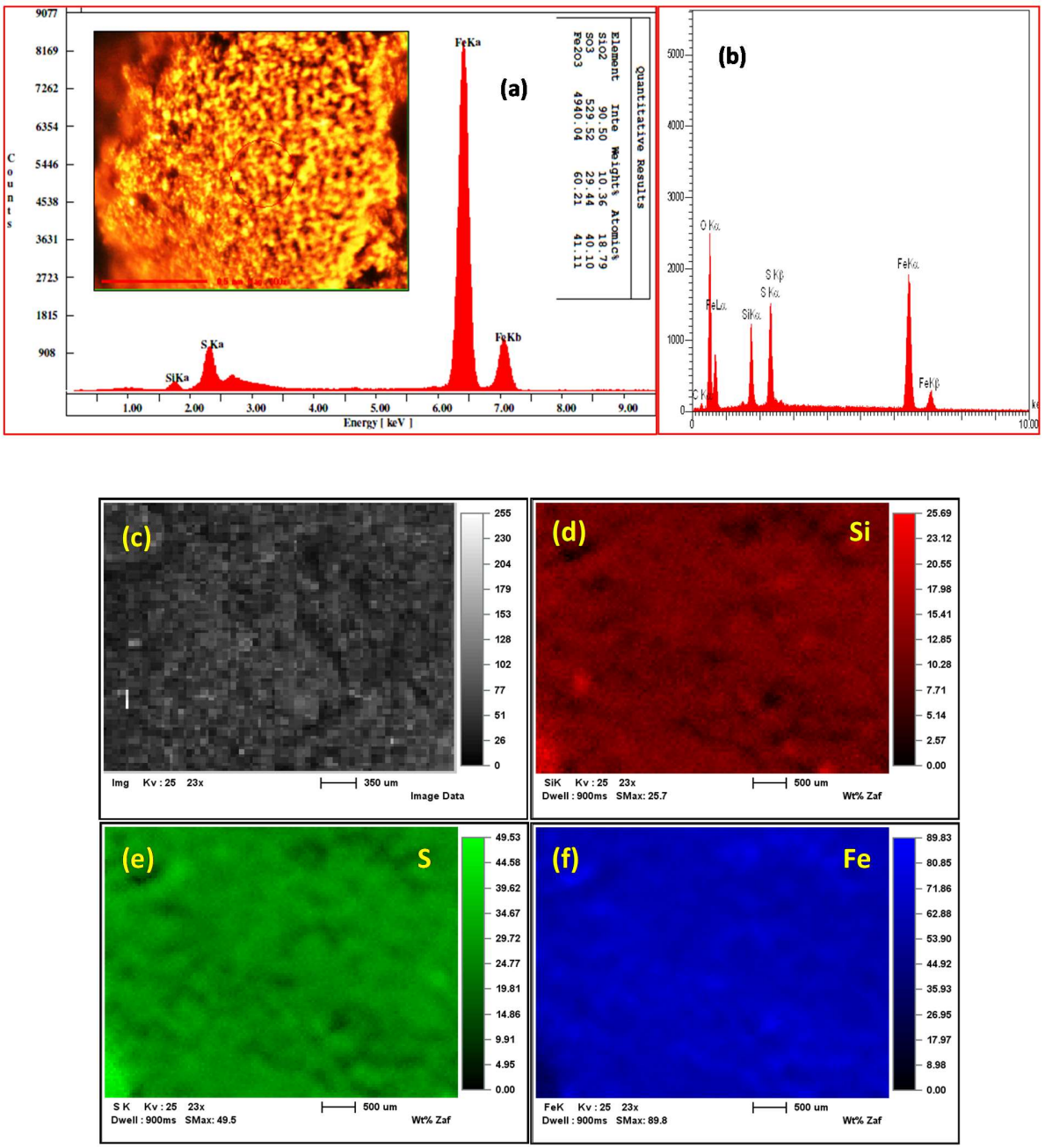

Fig. 5. (a) Micro X-ray fluorescence (μXRF) quantitative results (b) SEM-EDX (c) μXRF image and μXRF elemental mapping images of (d) silisium (red), (e) sulfur (green), (f) iron (blue) of nano catalyst [Fe_3O_4@SiO_2@$(CH_2)_3$S-SO_3H].

The particle size and shape as well as the morphology of nanoporous catalyst **2** were studied by XRD, SEM, and HRTEM (Figures 5-7 and Table 1). Characterization by X-ray diffraction (XRD) was performed to investigate the crystalline structure of [Fe_3O_4@SiO_2@$(CH_2)_3$S-SO_3H] in a range of $10 < 2\theta < 80°$ (Figure 5). On the other hand, XRD patterns demonstrated diffraction lines of high crystalline nature at 2θ = 18.00°, 30.30°, 35.50°, 43.60°, 54.00°, 57.30°, 62.70° and 74.60° corresponding to Fe_3O_4 diffraction lines (111), (220), (311), (400), (422), (511), and (440) (Figure 6) [24a]. The peaks in range of 20 to 29 are related to Si [25], indicating this shift a proper progress in the catalyst preparation. Furthermore, the average crystalline size D (nm) of **2** could be estimated according to the Scherrer equation $D = K\lambda/(\beta \cos \theta)$, where λ is the X-ray wavelength of Cu k_α (1.54Å), K is the Scherrer constant with a value of 0.9, β is the peak width at half maximum (FWHM) of the peak in radians, and θ is the Bragg diffraction angle. On the other hand, the averaged inter-planar distance [nm] of **2**, 0.49279 nm (sing the similar highest diffraction line at 18.0°), was calculated according to the Bragg equation: $dhkl = \lambda/(2\sin\theta)$, where K is a shape factor with the value of 0.9, θ is the Bragg diffraction angle, λ is the wavelength of Cu k_α (1.5405 Å) as the X-ray source. Crystalline sizes from various diffraction lines using the Scherrer equation were found to be in the nanometer range (29.06 - 47.31 nm), which is in a close agreement with the scanning electron microscopy (SEM) results.

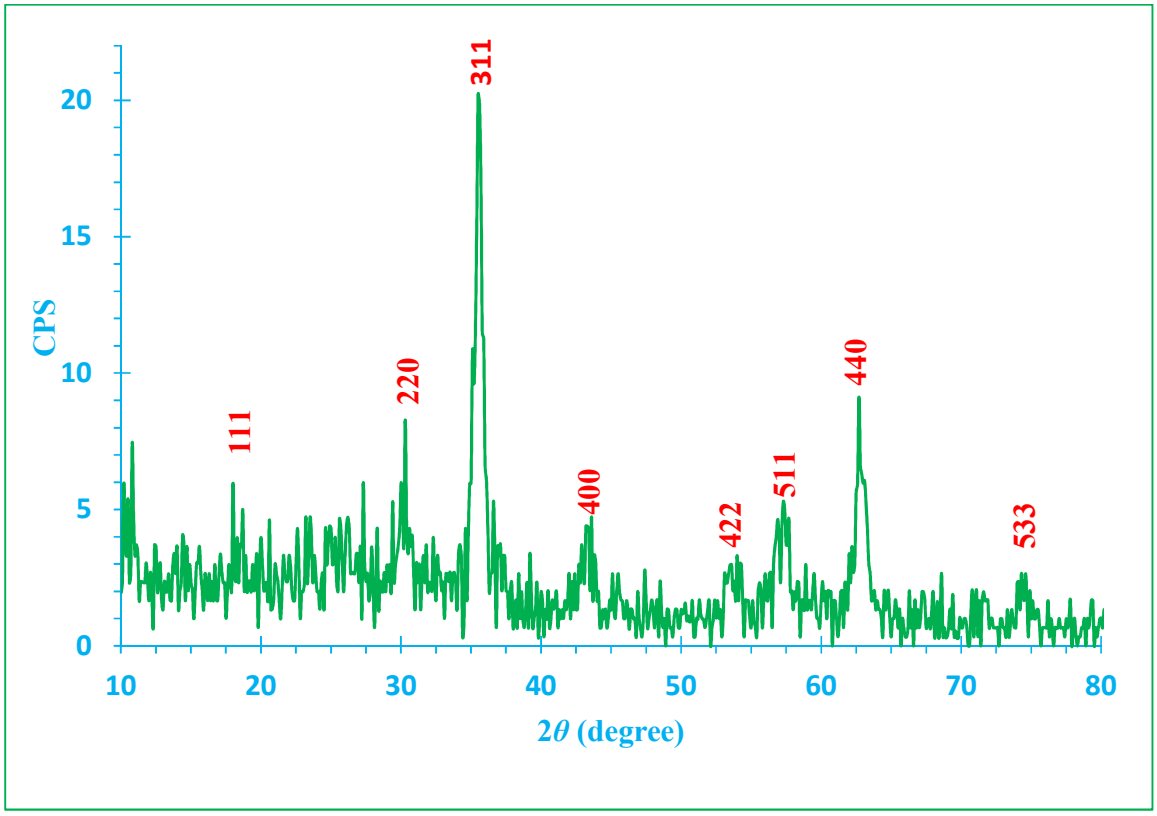

Fig. 6. XRD pattern of nano [Fe_3O_4@SiO_2@$(CH_2)_3$S-SO_3H]

Table 1. X-ray diffraction (XRD) data for nano catalyst [Fe_3O_4@SiO_2@$(CH_2)_3$S-SO_3H]

Entry	2θ	Peak width [degree]	Size [nm]	Inter planar distance [nm]
1	18.00	0.1	82.54	0.49279
2	30.30	0.1	84.4	0.29497
3	35.50	0.5	16.73	0.25286
4	43.60	0.1	87.81	0.20758
5	57.30	0.3	30.37	0.16078

6	62.70	0.1	95.46	0.14817
7	74.60	0.2	49.78	0.12721

Studies by SEM and HRTEM spectroscopy (Figure 7), helpful techniques to provide information about particle size and morphology of the materials, showed well-dispersed nanospherical particles with a high yield with an average size of 85 nm.

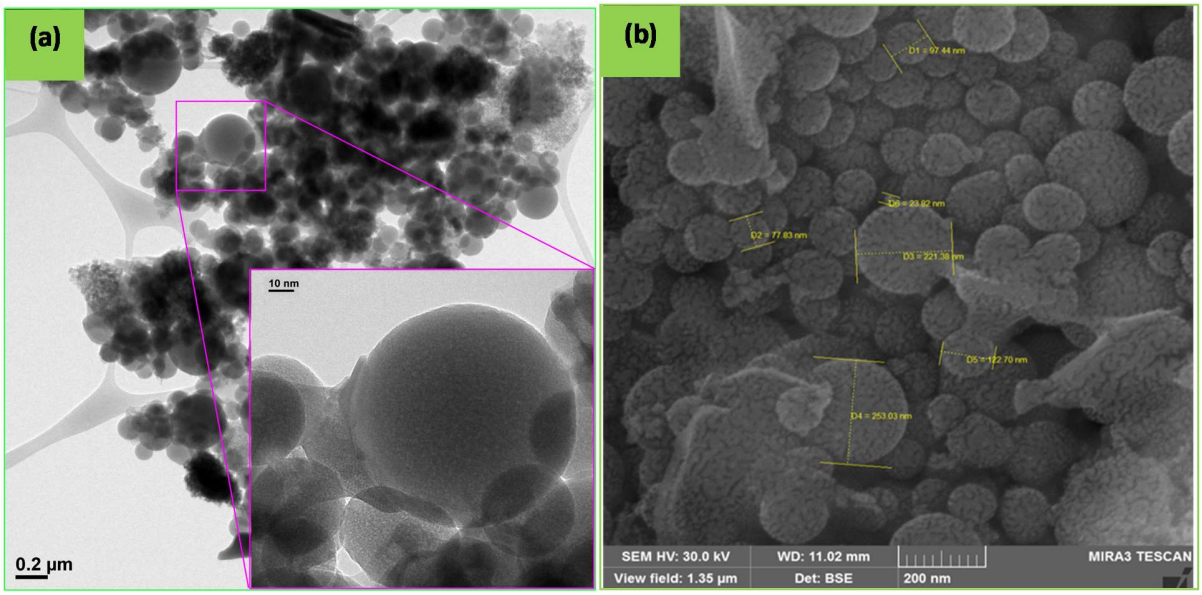

Fig. 7. (a) High resolution transmission electron microscopy (HRTEM) and (b) Scanning electron microscopy (SEM) of nano magnetic [Fe_3O_4@SiO_2@$(CH_2)_3$S-SO_3H]

Next, Nitrogen adsorption/desorption isotherm was carried out to obtain the information on the porosity and total surface area of the catalyst **2**. As shown in Figure 8a, the studied catalyst exhibited type II isotherm according to the IUPAC definition and with H_3 type hysteresis loop, which indicated the presence of a nanoporous structure. The surface area and pore volume of the catalyst are listed in Table 2. Moreover, a narrow pore-size distribution was calculated from the adsorption branch on the basis of BJH model (Figure 8b).

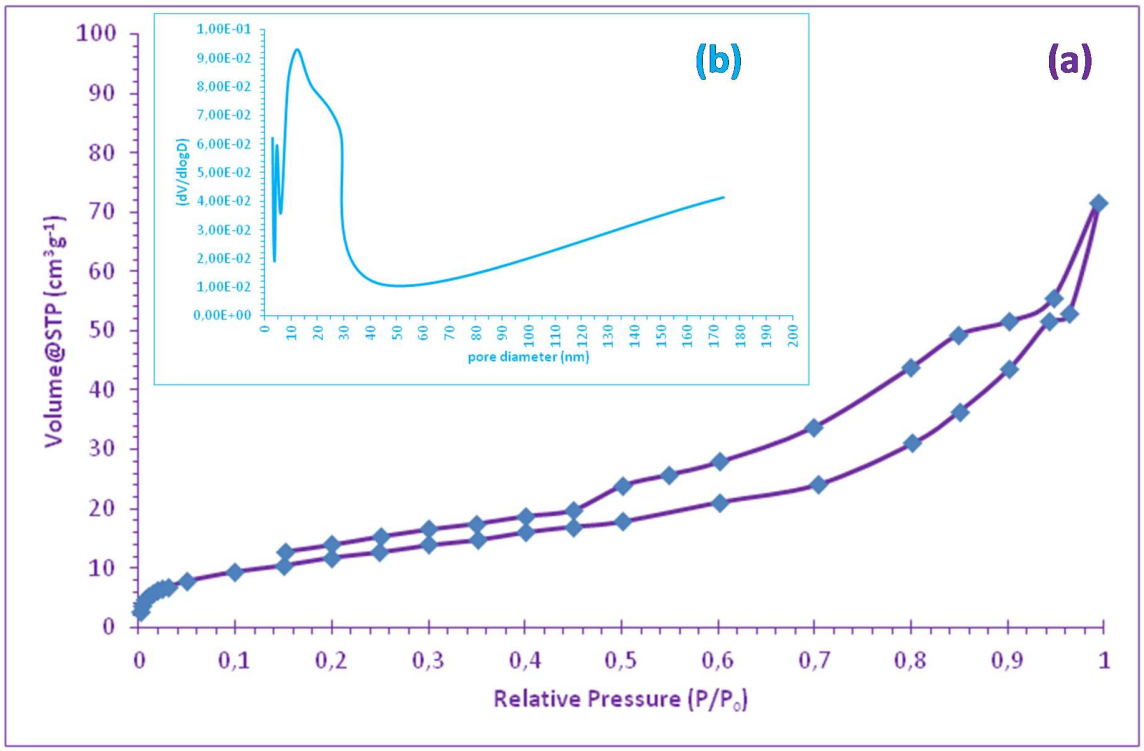

Fig. 8. (a) N_2 physisorption isotherm and (b) BJH pore size distribution of the [Fe_3O_4@SiO_2@$(CH_2)_3$S-SO_3H]

Table 2. Textural properties of the [Fe_3O_4@SiO_2@$(CH_2)_3$S-SO_3H]

S_{BET}[a] (m^2g^{-1})	S_{BJH}[b] (m^2g^{-1})	V_m[c] (cm^3g^{-1})	V_t[d] (cm^3g^{-1})	D[e] (nm)
44.36	31.56	0.10	0.08	3.05

[a] S_{BET}: total surface area. [b] S_{BJH}: surface area estimated by BJH model applied to the absorption branch of the isotherm. [c] V_m: mesopore volume. [d] V_t: total pore volume. [e] D: pore diameters estimated by BJH model applied to the absorption branch of the isotherm.

X-ray photoelectron spectroscopy (XPS) studies were next performed over [Fe_3O_4@SiO_2@$(CH_2)_3$S-SO_3H] in order to get insight about the surface composition and changes

associated with the chemical reaction of this catalyst (Figure 9). As expected, the peaks corresponding to S2p, O1s, C1s, Fe2p, and Si2p were clearly seen in the XPS survey spectrum of cat **2**, which confirmed a 3-(trimethoxysilyl)-1-propanethiol moiety covalently bonded to Fe_3O_4@SiO_2 (Figure 9a). As shown in Scheme 1, there are two types of sulfur containing groups, sulfide (-S-S-) as a covalent bridge bond and sulfate (-SO_3) as an active catalytic site. Therefore, the high resolution XPS spectrum of S2p was used as a potential technique for the analysis of both internal and terminal sulfurs on catalyst **2**. As shown in Figure 9b, the S2p spectrum comprises two singlet binding energy located at approximately 163.32 eV (S-S) and 168.88 eV (SO_3H) with a relative peak area ratio (1:5) respectively. Each S2p peak could be de-convoluted into the two different peaks located at approximately 163.32, 168.88 eV, corresponding to $2p^{3/2}$ and 164.838, 169.94 eV, which corresponded to $2p^{1/2}$ level. Interestingly, the relative area between S-S and S-O/S=O were not same indicating that the surface of catalysts was covered with thiosulfonate groups [25]. On the other hand, the XPS peak for chloride was not detected, (Figure 8b, orange lines), and only an orange residuals lines located at 522.68 eV were observed. Since the μXRF, EDX, and XPS had previously approved the presence of sulfur in the structure of catalyst, this result clearly suggested the absence of unreacted $ClSO_3H$ on the surface of the catalyst.

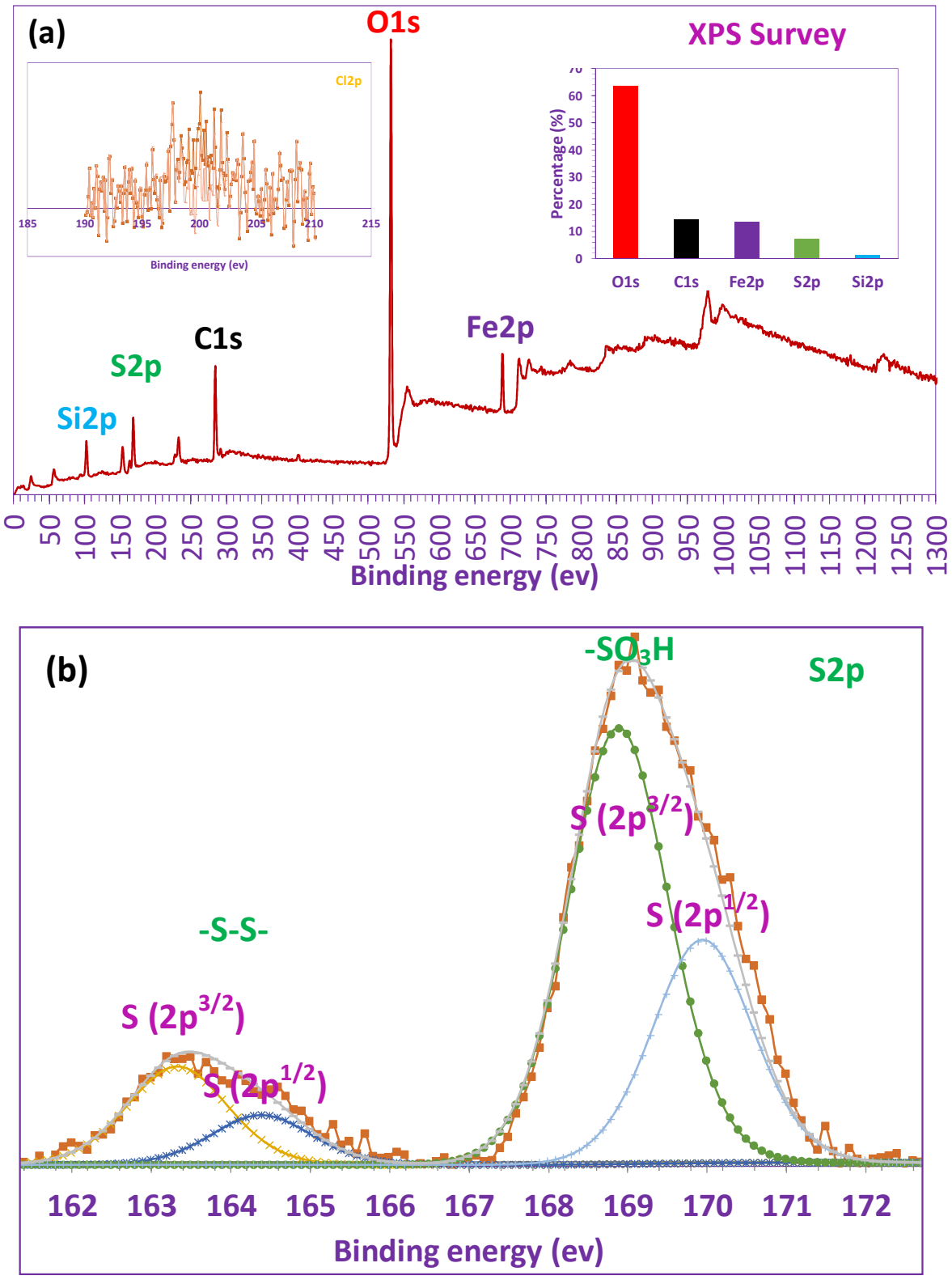

Fig. 9. XPS spectra of (a) Survey (inlet: Cl2p), and (b) S2p of nano catalyst **2**.

After characterization of the catalyst, we studied its use in the synthesis of pyrido[2,3-d]pyrimidines under nest conditions. Initially, an optimization of the reaction conditions (catalyst loading, temperature, and solvent) was carried out for the condensation between 4-nitrobenzaldehyde, malononitrile and 2,4-diamino-6-hydroxypyrimidine at 100 ºC. As shown in Table 3, the best results were obtained when the reaction was performed in the presence of 2 mg of the catalyst (Table 3, entry 1). No yield improvement was observed using higher catalyst loadings (Table 3, entries 2 to 6). Table 3 clearly displays that in the absence of catalyst and different temperature 25 and 100 ºC, the product was produced in low yields (Table 3, entry 7 and 8). In addition, keeping the catalyst loading at 2 mg, lowers temperatures led to lower reaction yields (Table 3, entry 9 to 11).

Table 3. Condensation of 4-nitrobenzaldehyde, malononitrile and 2,4-diamino-6-hydroxypyrimidine under neat conditions. Catalyst loading and temperature study.[a]

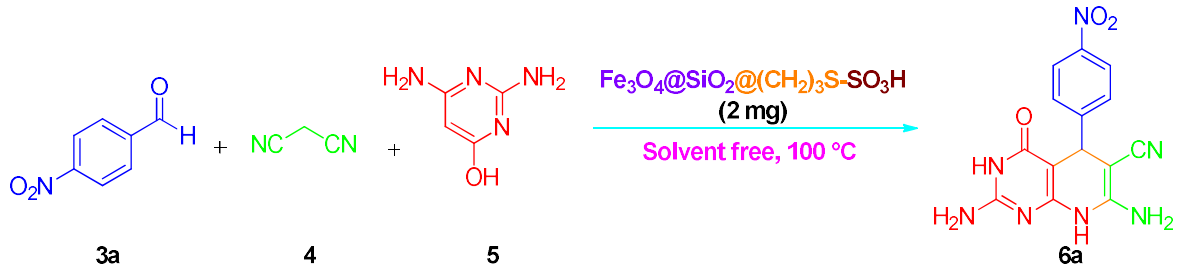

3a 4 5 6a

Entry	Catalyst loading (mg)	Temperature (°C)	Time (min)	Yield[b] (%)
1	2	100	20	92
2	2.5	100	22	92
3	10	100	20	90
4	30	100	25	87

To	5	50	100	20	80
	6	70	100	20	75
	7	-	110	180	20
	8	-	25	300	5
	9	2	25	120	20
	10	2	50	60	55
	11	2	80	60	90

[a]Reaction conditions: 4-nitrobenzaldehyde (1 mmol; 151 mg), malononitrile (1 mmol, 66 mg) and 2,4-diamino-6-hydroxypyrimidine (1 mmol, 126 mg); [b]Isolated yield.

compare the effect of the solution in comparison with solvent-free conditions, a mixture of 4-nitrobenzaldehyde, malononitrile and 2,4-diamino-6-hydroxypyrimidine as a typical reaction, by using 2 mg of nano [Fe_3O_4@SiO_2@$(CH_2)_3$S-SO_3H] as a catalyst in a good range of solvents such as H_2O, MeCN, EtOH, EtOAC and CH_2Cl_2 were investigated under reflux condition. The results are summarized in Table 4. The results display that solvent-free condition was the best of choice for this reaction (Table 4, entry 6).

Table 4. The effect of various solvents in the presence of 2 mg of [Fe_3O_4@SiO_2@$(CH_2)_3$S-SO_3H] as a catalyst in the one-pot condensation reaction of 4-nitrobenzaldehyde, malononitrile and 2,4-diamino-6-hydroxypyrimidine.[a]

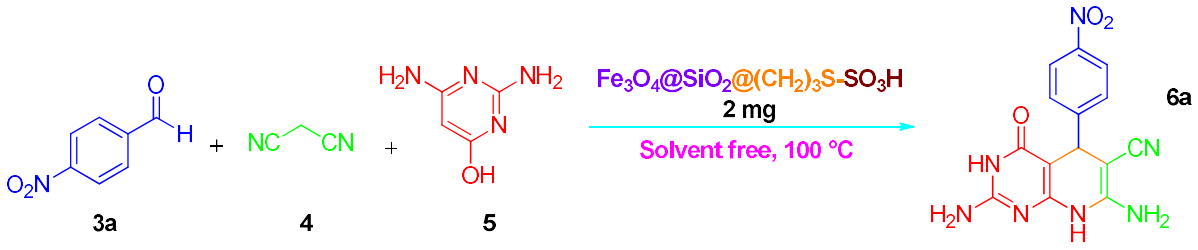

Entry	Solvent	Temperature	Time	Yield[b] (%)

1	EtOAC	Reflux	120	60
2	MeCN	Reflux	90	78
3	EtOH	Reflux	90	65
4	CH_2Cl_2	Reflux	150	50
5	H_2O	Reflux	60	90
6	-	Reflux	20	92

Reaction condition: [a]4-nitrobenzaldehyde (1 mmol; 151 mg), malononitrile (1 mmol, 66 mg) and 2,4-diamino-6-hydroxypyrimidine (1 mmol, 126 mg); [b]Isolated yield.

After optimization of the reaction conditions, the efficiency and applicability of the method were studied via the reaction of malononitrile and 2,4-diamino-6-hydroxypyrimidine with various aromatic aldehydes in the presence of nano [Fe_3O_4@SiO_2@$(CH_2)_3$S-SO_3H]. The results are summarized in Table 5. Generally, all tested aldehydes including benzaldehyde as well as other aromatic aldehydes substituted with electron-donating and electron withdrawing groups afforded the desired pyrido[2,3-*d*]pyrimidine derivatives in good to excellent yields (84-94%) in short reaction times (8-23 min).

Table 5. Synthesis of pyrido[2,3-*d*]pyrimidine derivatives under neat conditions at 100°C.[a]

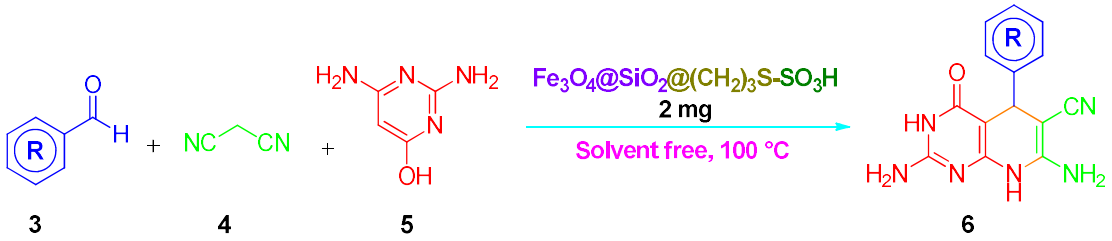

3 4 5 6

Entry	Product	Time (min)	Yield (%)[b]	M.p (°C)

					Found and [Lit.][Ref.]
1	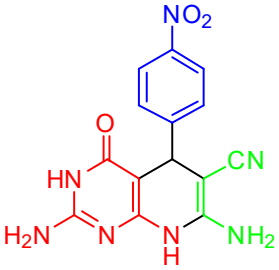	**6a**	13	87	209-211 [>300][12]
2	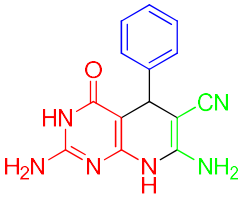	**6b**	18	90	216-218 [-]
3	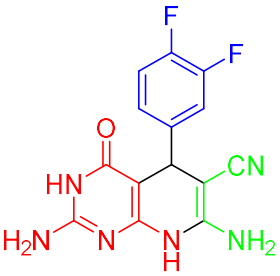	**6c**	13	92	213-215 [-]
4	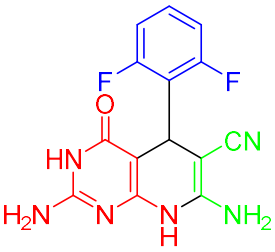	**6d**	8	94	272-274 [-]
5	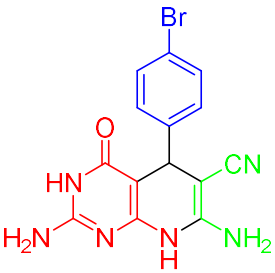	**6e**	11	92	227-229 [>300][12]

6	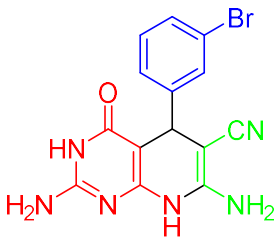	**6f**	12	90	229-231 [-]
7	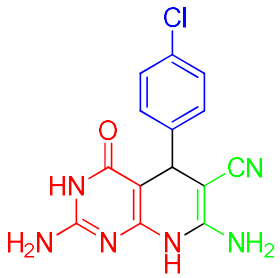	**6g**	10	91	220-222 [-][12]
8	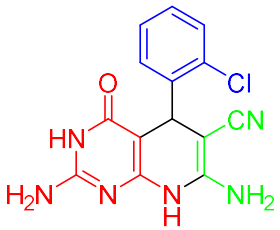	**6h**	14	89	235-237 [>300][12]
9	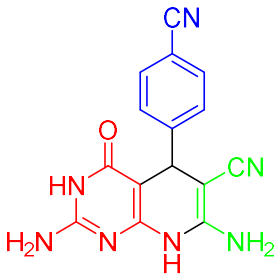	**6i**	13	91	236-238 [-]
10	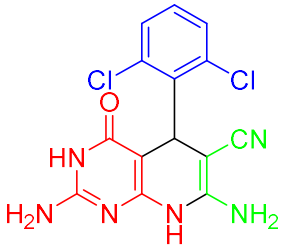	**6j**	12	90	266-268 [-]

11	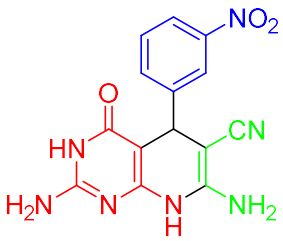	**6k**	16	89	233-235 [>300][12]
12	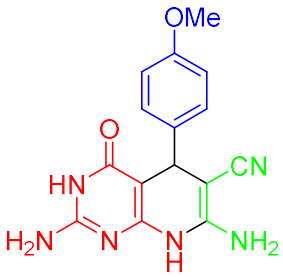	**6l**	19	86	205-207 [-]
13	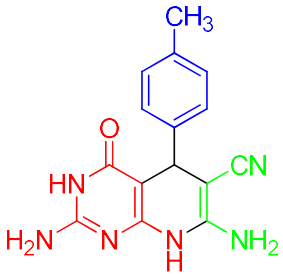	**6m**	17	84	223-225 [>300][12]
14	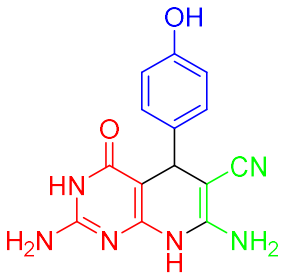	**6n**	22	86	164-166 [-]

15	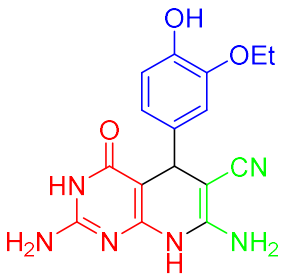	**6o**	20	89	205-207 [-]
16	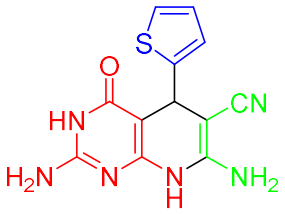	**6p**	23	86	213-215 [-]

[a]Reaction conditions: arylaldehydes (1 mmol), malononitrile (1 mmol, 66 mg), 2,4-diamino-6-hydroxypyrimidine(1 mmol, 126 mg) and [Fe_3O_4@SiO_2@$(CH_2)_3$S-SO_3H] (2 mg). [b] Isolated yield.

A mechanistic proposal for the **2**-catalyzed route towards the synthesis of pyrido[2,3-*d*]pyrimidine derivatives has been summarized in Scheme 3. According to the XPS results and previous works [12], the aldehyde, which is initially activated by the acidic surface sites of nano [Fe_3O_4@SiO_2@$(CH_2)_3$S-SO_3H], suffer a Knoevenagel condensation with malononitrile to give intermediate **A**. Then, this excellent Michael acceptor undergoes a conjugate addition reaction by 2,4-diamino-6-hydroxypyrimidine to afford intermediate **B** that, after a **2**-promoted intramolecular cyclization and a final tautomerization, affords the corresponding compounds **6** (Scheme 3).

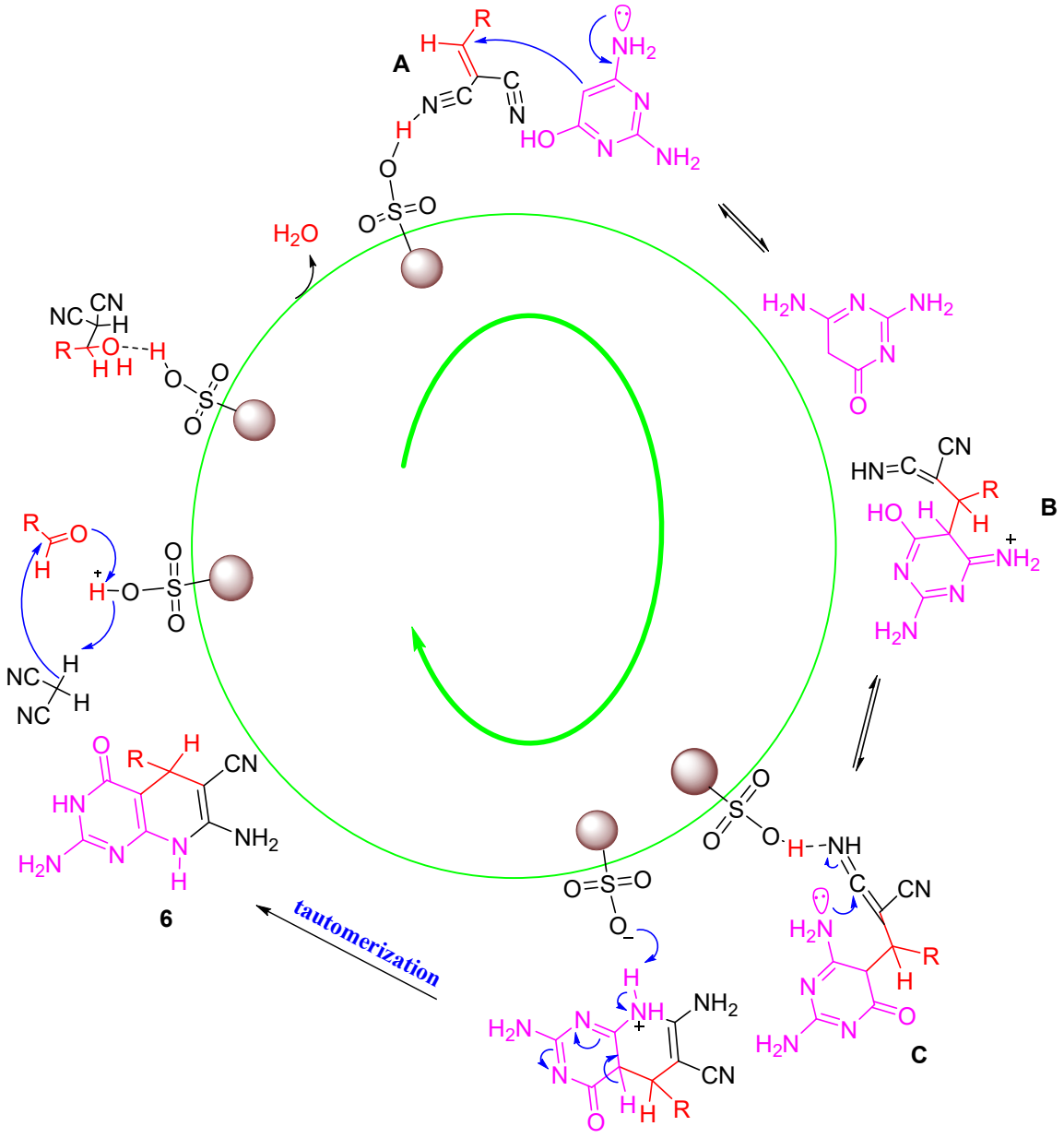

Scheme 3. Proposed mechanism for the synthesis of pyrido[2,3-*d*]pyrimidines in the presence of [Fe_3O_4@SiO_2@$(CH_2)_3$S-SO_3H].

Catalyst recycling and recovering is an essential consideration regarding environmental, economic and industrial considerations. Apart from the magnetic isolation and separation of the catalyst upon reaction completion, the additional possibility to reuse it in several reaction cycles on the model

synthesis of **6a** was also studied. Thus, after each cycle, the catalyst was magnetically separated from the reaction mixture and washed with a hot ethanol-water mixture and then, reused. As seen in Figure 10, the described catalyst can be reused up to 8 times without an important loss of activity.

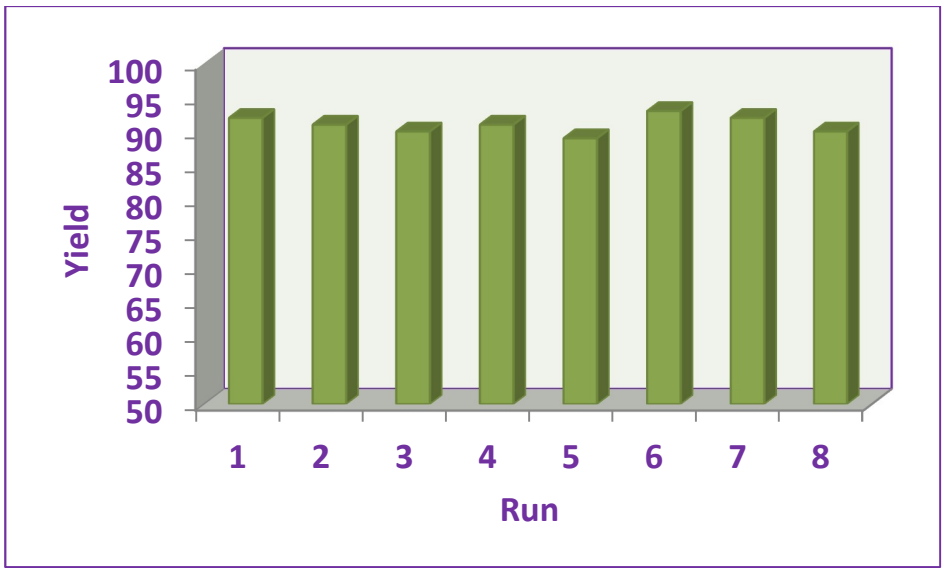

Fig. 10. Recyclability of nano[Fe_3O_4@SiO_2@$(CH_2)_3$S-SO_3H] in the synthesis **6a** under neat conditions at 100 °C.

Conclusion

In conclusion, we have described the first catalytic synthesis of pyrido[2,3-*d*]pyrimidines using the novel and recoverable nano magnetic [Fe_3O_4@SiO_2@$(CH_2)_3$S-SO_3H] catalyst which has been fully characterized. The major advantages of this methodology are high yields, short reaction times, and reusability of the catalyst. The described results from this research supports the idea of rational designs, syntheses and applications of tasked-specific and reusable catalysts for the synthesis of polynitrogenated heterocyclic compounds containing the 1,4-dihydropyridine moietie.

2. Experimental

2.1. General information

Solvents and reagents were used as obtained from Sigma-Aldrich, Alfa Aesar, and Merck companies without further purification. Progress of the reactions was monitored by TLC using silica gel SIL G/UV 254 plates. R_f values were measured using EtOAc as solvent. Melting points were recorded on a Büchi B-545 apparatus in open capillary tubes. Fourier transformed infrared (FTIR) spectra of the catalyst and the synthesized products were recorded on a FTIR spectrometer Perkin-Elmer spectrum 65 using KBr disks. High resolution mass spectra (GC/QTOF, EI, 70 eV) were obtained using an Agilent 7200 Network spectrometer,. ^{1}H NMR (300 and 400 MHz) spectra were obtained on a Bruker Avance 300 and a Bruker Avance 400 NMR spectrometers, under proton coupled mode using deuterated DMSO as a solvent, unless otherwise stated. ^{13}C NMR (101 MHz) spectra were acquired on a Bruker Avance 400 NMR spectrometer in the proton decoupled mode at 20 °C in deuterated DMSO as solvent, unless otherwise stated. Chemical shifts are given in δ (parts per million) and the coupling constants (*J*) in Hertz. ^{19}F NMR (282 MHz) spectra were recorded on a Bruker Avance 300 NMR spectrometer, in proton coupled mode. Data for ^{1}H NMR spectra is reported as follows: chemical shift (ppm), multiplicity (s, singlet; d, doublet; t, triplet; q, quartet; m, multiplet; and br., broad), coupling constant (Hz), and integration. Thermogravimetric analyses (TGA) were carried out on a Mettler Toledo equipment (model TGA/SDTA851 and /SF/1100 TGDTA) under nitrogen atmosphere at 25°C and using a heating rate of 25 °C min^{-1} up to 700 °C. Powder X-ray diffraction (XRD) pattern was recorded with an Ital structure ADD2000 model, using a monochromatized Cu Kα (λ = 0.154 nm) X-ray source in the range $10° < 2\theta < 80°$. High resolution transmission electron microscopy (HRTEM) images were obtained using a JEOL JEM-2010 microscope operating at an accelerating voltage of 200 kv. Sample was prepared by drop casting the dispersed particles onto a 200-mesh copper grid coated with a holey carbon film. Scanning electron microscopy (SEM) studies were performed using a TESCAN/MIRA with a

maximum acceleration voltage of the primary electrons between 10 and 15 kV. N_2 adsorption-desorption isotherms were measured at 77 K with a Quantachrome NOVA 4000e analyzer. The Brunauer-Emmett-Teller (BET) method was used to calculate the specific surface areas (S_{BET}). By using the Barrett-Joyner-Halenda (BJH) model, the pore volumes and pore size distributions were derived from the adsorption branches of isotherms. The micropore surface area (S_{BET} micro) was calculated using the *V-t* plot method. X-ray photoelectron spectroscopy (XPS, K-ALPHA, Thermo Scientific) was used to analyze the samples surface. All spectra were collected using Al-K radiation (1486.6 eV), monochromatized by a twin crystal monochromator, yielding a focused X-ray spot (elliptical in shape with a major axis length of 400μm) at 3 mA × 12 kV. XPS data were analyzed using Thermo Scientific Avantage Software. A smart background function was used to approximate the experimental backgrounds and surface elemental composition was calculated from background-subtracted peak areas. Charge compensation was achieved with the system flood gun that provides low energy electrons and low energy argon ions from a single source. A Gaussian/Lorenzian product function peak shape model (L/G Mix (%) = 30) was used. Micro X-ray fluorescence (μXRF) analyses were performed on an Edax, Orbis using 25 kV with image mapping resolution (128 × 100).

Prapration of nano[Fe_3O_4@SiO_2@$(CH_2)_3$S-SO_3H] catalyst

Initially, iron oxide (Fe_3O_4) magnetic nanoparticles and the silica coated on iron oxide (Fe_3O_4@SiO_2) were synthesized according to previously reported procedures [24]. Thus, in a round-bottomed flask, 1.0 g of previously dried (under vacuum) silica coated magnetic nanoparticles was dispersed in 50 mL of anhydrous toluene and it was sonicated for 30 min. After this time, 3.5 mL of 3-(trimethoxysilyl)-1-propanethiol were added dropwise to the suspended solid nanoparticles, being the obtained mixture refluxed under mechanical stirring

for 24 h. After this time, the prepared nanoparticles **1** were isolated by using an external magnet and dried at room temperature. Then, in a round-bottomed flask, 1.0 g of [Fe_3O_4@SiO_2@$(CH_2)_3SH$] (**1**) was sonicated for 30 min in anhydrous CH_2Cl_2 (50 mL). Next, 0.5 mL of cholorosulfunic acid were added dropwise to the reaction mixture at room temprature and the resulting solution was allowed to stirr for 2 h until no more hydrogen chloride evolution was detected. Then, the resulting mixture was isolated by using an external magnet to afford [Fe_3O_4@SiO_2@$(CH_2)_3$S-SO_3H] (**2**) which was washed with ethanol and dried at room temperature (Scheme 1).

General procedure for the synthesis of pyrido[2,3-*d*]pyrimidine derivatives

In a 10 mL round-bottomed flask, a mixture of aldehyde (1 mmol), malononitrile (1 mmol, 66 mg), 2,4-diamino-6-hydroxypyrimidine (1 mmol, 126 mg), and [Fe_3O_4@SiO_2@$(CH_2)_3$S-SO_3H] (2 mg) were stirred at 100 °C under neat conditions. After completion of the reaction (monitored by TLC), the mixture was allowed to cool to room temperature. Then, the resulted solid mixture was solved in DMF and the catalyst was recovered using a magnet. Products precipitated out of the DMF solution. Finally, the obtained crystals were washed with water to remove DMF (Table 1) (Scheme 2).

2,7-Diamino-5-(4-nitrophenyl)-4-oxo-3,4,5,8-tetrahydropyrido[2,3-*d*]pyrimidine-6-carbonitrile (6a**):**

Isolated as yellow solid, (283 mg, 87%), R_f: 0.16, Melting point: 209 – 211 °C; FT-IR: υ (cm^{-1}) = 3471, 3385, 3348, 3167, 2191, 1666, 1630, 1555, 1516, 1455, 1394, 1346, 1204; ^{1}H NMR: δ 8.19 (d, *J* = 8.7, 2H), 7.45 (d, *J* = 8.7, 2H), 7.08 (br. s, 2H), 6.27 (br. s, 2H), 6.17 (br. s, 2H), 4.62 (s, 1H); ^{13}C NMR: δ 163.2, 162.4, 162.2, 160.5, 152.8, 146.8, 128.7, 124.2, 120.4, 84.5, 57.1, 35.7; HRMS calcd. for $C_{10}H_5N_3O_2$ [M^+ - ($C_4H_6N_4O$)] 199.0382, found 199.0383.

2,7-Diamino-4-oxo-5-phenyl-3,4,5,8-tetrahydropyrido[2,3-*d*]pyrimidine-6-carbonitrile (6b**):**

Isolated as khaki solid, (252 mg, 90%), R_f: 0.65, Melting point: 216 – 218 °C; FT-IR: υ (cm^{-1}) = 3491, 3384, 3169, 2183, 1662, 1465, 1394, 1201, 1132; ^{1}H NMR: δ 7.33 – 7.26 (m, 2H), 7.25 – 7.17 (m, 3H), 6.91 (br. s, 2H), 6.15 (br. s, 2H), 6.09 (br. s, 2H), 4.41 (s, 1H); ^{13}C NMR (75 MHz) δ 163.2, 162.1 (2c), 160.3, 145.2, 128.9, 127.4, 127.2, 120.8, 85.7, 58.6, 35.9; HRMS calcd. for $C_{10}H_6N_2$ [M^+ - ($C_4H_6N_4O$)] 154.0531, found 154.0537.

2,7-Diamino-5-(3,4-difluorophenyl)-4-oxo-3,4,5,8-tetrahydropyrido[2,3-*d*]pyrimidine-6-carbonitrile (6c**):**

Isolated as lemon chiffon solid, (290 mg, 92%), R_f: 0.30, Melting point: 213 – 215 °C; FT-IR: υ (cm^{-1}) = 3480, 3403, 3328, 3154, 2929, 2185, 1656, 1634, 1556, 1459, 1395, 1286, 1140, 799; ^{1}H NMR: δ 7.43 – 7.32 (m, 1H), 7.26 – 7.17 (m, 1H), 7.11 – 6.90 (m, 3H), 6.23 (br. s, 2H), 6.14 (br. s, 2H), 4.45 (s, 1H); ^{13}C NMR: δ 163.1, 162.3, 162.0, 160.4, 149.50 (dd, *J* = 246.0, 12.8 Hz), 148.65 (dd, *J* = 245.0, 12.6 Hz), 143.0 (t, *J* = 3.5), 124.0 (m), 120.6, 118.0 (d, *J* = 17.1), 116.0 (d, *J* = 17.1), 84.9, 57.7, 35.2; ^{19}F NMR: δ -136.58 (d, *J* = 22.5 Hz), -139.17 (d, *J* = 22.5 Hz); HRMS calcd. for $C_{10}H_4F_2N_2$ [M^+ - ($C_4H_6N_4O$)] 190.0343, found 190.0344.

2,7-Diamino-5-(2,6-difluorophenyl)-4-oxo-3,4,5,8-tetrahydropyrido[2,3-*d*]pyrimidine-6-carbonitrile (6d**):**

Isolated as floral white solid, (297 mg, 94%), R_f: 0.20, Melting point: 272 – 274 °C; FT-IR: υ (cm^{-1}) = 3478, 3377, 3181, 2193, 1665, 1621, 1469, 1392, 1208, 995, 782, 563; ^{1}H NMR: δ 7.41 – 7.28 (m, 1H), 7.17 – 6.93 (m, 4H), 6.18 (br. s, 2H), 5.75 (br. s, 2H), 4.89 (s, 1H); ^{13}C NMR: δ 163.1, 162.3, 162.2 (dd, *J* = 240, 20), 161.3, 154.5, 129.8 (t, *J* = 10.6), 120.4, 119.0 (t, *J* = 15.9), 112.4 (d, *J* = 24.7), 83.4, 54.2, 26.2; ^{19}F NMR (282 MHz) δ -106.83, -114.09; HRMS calcd. for $C_{10}H_4F_2N_2$ [M^+ - ($C_4H_6N_4O$)] 190.0343, found 190.0350.

2,7-Diamino-5-(4-bromophenyl)-4-oxo-3,4,5,8-tetrahydropyrido[2,3-*d*]pyrimidine-6-carbonitrile (6e**):**

Isolated as moccasin solid, (329 mg, 92%), R_f: 0.16, Melting point: 227 – 229 °C; FT-IR: υ (cm^{-1}) = 3466, 3391, 3173, 2184, 1661, 1625, 1553, 1384, 1298, 1132; ^{1}H NMR: δ 7.53 – 7.47 (m, 2H), 7.19 – 7.12 (m, 2H), 6.97 (br. s, 2H), 6.20 (br. s, 2H), 6.12 (br. s, 2H), 4.43 (s, 1H); ^{13}C NMR: δ 163.1, 162.2, 162.1, 160.3, 144.6, 131.7, 129.7, 120.7, 120.2, 85.2, 57.9, 35.4; HRMS calcd. for $C_{10}H_5BrN_2$ [M^+ - ($C_4H_6N_4O$)] 231.9636 and 233.9616, found 231.9645 and 233.9620.

2,7-Diamino-5-(3-bromophenyl)-4-oxo-3,4,5,8-tetrahydropyrido[2,3-*d*]pyrimidine-6-carbonitrile (6f**):**

Isolated as linen solid, (323 mg, 90%), R_f: 0.30, Melting point: 229 – 231 °C; FT-IR: υ (cm^{-1}) = 3491, 3381, 3182, 2193, 1668, 1619, 1553, 1448, 1388, 1295, 1130, 1070, 786; ^{1}H NMR: δ 7.45 – 7.38 (m, 2H), 7.28 (t, *J* = 7.9, 1H), 7.16 (d, *J* = 7.5, 1H), 7.01 (br. s, 2H), 6.25 (br. s, 2H), 6.15 (br. s, 2H), 4.43 (s, 1H); ^{13}C NMR: δ 163.1, 162.3, 162.1, 160.4, 148.0, 131.2, 130.1 (2c), 126.5, 122.0, 120.6, 85.0, 57.8, 35.5; HRMS calcd. for $C_{10}H_5BrN_2$ [M^+ - ($C_4H_6N_4O$)] 231.9636 and 233.9616, found 231.9638 and 233.9615.

2,7-diamino-5-(4-chlorophenyl)-4-oxo-3,4,5,8-tetrahydropyrido[2,3-d]pyrimidine-6-carbonitrile (6g**):**

Isolated as khaki solid, (mg, 91%), R_f: 0.65, Melting point: 220 – 222 °C; FT-IR: υ (cm^{-1}) = 3492, 3379, 3331, 3178, 2929, 2194, 1669, 1618, 1552, 1449, 1391, 1297, 1131, 828; ^{1}H NMR: δ 7.40 – 7.33 (m, 2H), 7.25 – 7.18 (m, 2H), 6.96 (br. s, 2H), 6.19 (br. s, 2H), 6.12 (br. s, 2H), 4.44 (s, 1H); ^{13}C NMR: δ 163.1, 162.2, 162.1, 160.3, 144.2, 131.7, 129.3, 128.8, 120.7, 85.2, 58.0, 35.3; HRMS calcd. for $C_{10}H_5ClN_2$ [M^+ - ($C_4H_6N_4O$)] 188.0141 and 190.0112, found 188.0145 and 190.0113.

2,7-Diamino-5-(2-chlorophenyl)-4-oxo-3,4,5,8-tetrahydropyrido[2,3-*d*]pyrimidine-6-carbonitrile (6h**):**

Isolated as papaya whip solid, (279 mg, 89%), R_f: 0.40, Melting point: 235 – 237 °C; FT-IR: υ (cm^{-1}) = 3473, 3395, 3322, 3165, 2191, 1666, 1629, 1558, 1456, 1394, 1299, 1138, 1035, 750; ^1H NMR: δ 7.41 – 7.23 (m, 4H), 6.97 (br. s, 2H), 6.15 (br. s, 2H), 5.74 (br. s, 2H), 4.76 (s, 1H); ^{13}C NMR (75 MHz) δ 163.1, 162.2 (2c), 160.6, 140.7, 132.4, 131.4, 130.6, 129.3, 128.1, 120.3, 84.3, 56.1, 35.2; HRMS calcd. for $C_{10}H_5ClN_2$ [M^+ - ($C_4H_6N_4O$)] 188.0141 and 190.0112, found 188.0145 and 190.0112.

2,7-Diamino-5-(4-cyanophenyl)-4-oxo-3,4,5,8-tetrahydropyrido[2,3-*d*]pyrimidine-6-carbonitrile (6i**):**

Isolated as khaki solid, (277 mg, 91%), R_f: 0.17, Melting point: 236 – 238 °C; FT-IR: υ (cm^{-1}) = 3451, 3413, 3337, 3204, 2885, 2731, 2227, 1633, 1594, 1442, 1395, 817; ^1H NMR: δ 10.06 (br. s, 1H), 7.89 – 7.72 (m, 4H), 6.49 (br. s, 2H), 6.38 – 6.15 (m, 3H), 4.72 (d, *J* = 11.5, 1H); ^{13}C NMR: δ 163.2, 162.6, 154.6, 145.6, 132.6, 129.2, 119.2, 114.9, 114.6, 110.6, 84.3, 42.6, 25.9; HRMS calcd. for $C_{11}H_5N_3$ [M^+ - ($C_4H_6N_4O$)] 179.0483, found 179.0486.

2,7-Diamino-5-(2,6-dichlorophenyl)-4-oxo-3,4,5,8-tetrahydropyrido[2,3-*d*]pyrimidine-6-carbonitrile (6j**):**

Isolated as white solid, (314 mg, 90%), R_f: 0.22, Melting point: 266 – 268 °C; FT-IR: υ (cm^{-1}) = 3479, 3377, 3319, 3181, 2193, 1670, 1621, 1469, 1394, 1208, 995, 782; ^1H NMR: δ 7.55 (d, *J* = 7.8, 1H), 7.44 (d, *J* = 7.8, 1H), 7.35 (t, *J* = 8.0, 1H), 7.05 (s, 2H), 6.20 (s, 2H), 5.42 (br. s, 2H), 5.32 (s, 1H); ^{13}C NMR δ 162.8, 162.3, 161.2, 135.8, 134.7, 131.8, 130.3, 129.2, 119.8, 82.7, 53.1, 33.6; HRMS calcd. for $C_{10}H_4Cl_2N_2$ [M^+ - ($C_4H_6N_4O$)] 221.9752 and 223.9722 and 225.9693 found 221.9754 and 223.9720 and 225.9694.

2,7-Diamino-5-(3-nitrophenyl)-4-oxo-3,4-dihydropyrido[2,3-*d*]pyrimidine-6-carbonitrile (6k**):**

Isolated as pale golden rod solid, (287 mg, 89%), R_f: 0.16, Melting point: 233 – 235 °C; FT-IR: υ (cm^{-1}) = 3496, 3466, 3400, 3121, 2917, 2187, 1674, 1634, 1594, 1536, 1351, 1148, 787; ^{1}H NMR: δ 8.18 – 8.05 (m, 2H), 7.72 – 7.52 (m, 2H), 7.08 (br. s, 2H), 6.31 (br. s, 2H), 6.17 (br. s, 2H), 4.63 (s, 1H); ^{13}C NMR: δ 163.1, 162.4, 162.2, 160.6, 148.1, 147.6, 134.2, 130.6, 122.4, 121.9, 120.5, 84.7, 57.4, 35.5; HRMS calcd. for $C_{10}H_5N_3O_2$ [M^+ - ($C_4H_6N_4O$)] 199.0382, found 199.0383.

2,7-Diamino-5-(4-methoxyphenyl)-4-oxo-3,4,5,8-tetrahydropyrido[2,3-*d*]pyrimidine-6-carbonitrile (6l**):**

Isolated as yellow solid, (266 mg, 86%), R_f: 0.29, Melting point: 205 – 207 °C; FT-IR: υ (cm^{-1}) = 3400, 2186, 1659, 1626, 1556, 1455, 1384, 1034; ^{1}H NMR: δ 7.11 (d, *J* = 8.7, 2H), 6.87 – 6.83 (m, 4H), 6.11 (br. s, 2H), 6.06 (br. s, 2H), 4.35 (s, 1H), 3.72 (s, 3H); ^{13}C NMR: δ 163.1, 162.1, 161.9, 160.1, 158.5, 137.3, 128.5, 120.8, 114.2, 85.9, 58.8, 55.5, 35.1; HRMS calcd. for $C_{11}H_8N_2O$ [M^+ - ($C_4H_6N_4O$)] 184.0637, found 184.0638.

2,7-Diamino-4-oxo-5-(*p*-tolyl)-3,4,5,8-tetrahydropyrido[2,3-*d*]pyrimidine-6-carbonitrile (6m**):**

Isolated as ivory solid, (247 mg, 84%), R_f: 0.18, Melting point: 223 – 225 °C; FT-IR: υ (cm^{-1}) = 3473, 3399, 3321, 3165, 2193, 2175, 1655, 1625, 1456, 1392, 1297, 1199, 1039, 792; ^{1}H NMR: δ 7.09 (s, 4H), 6.87 (s, 2H), 6.10 (br. s, 2H), 6.07 (br. s, 2H), 4.36 (s, 1H), 2.25 (s, 3H); ^{13}C NMR: δ 163.2, 162.1, 162.0, 160.1, 142.2, 136.3, 129.4, 127.4, 120.8, 85.8, 58.7, 35.6, 21.1; HRMS calcd. for $C_{11}H_8N_2$ [M^+ - ($C_4H_6N_4O$)] 168.0687, found 168.0684.

2,7-Diamino-5-(4-hydroxyphenyl)-4-oxo-3,4,5,8-tetrahydropyrido[2,3-*d*]pyrimidine-6-carbonitrile (6n**):**

Isolated as papaya whip solid, (254 mg, 86%), R_f: 0.23, Melting point: 164 – 166 °C; FT-IR: υ (cm^{-1}) = 3446, 3345, 3184, 2195, 1660, 1618, 1552, 1463, 1388, 1260, 664; ^{1}H NMR: δ 9.28 (br. s, 1H), 6.99 (d, *J* = 8.5, 2H), 6.82 (br. s, 2H), 6.67 (d, *J* = 8.5, 2H), 6.05 (br. s, 4H), 4.28 (s, 1H); ^{13}C NMR: δ 163.1, 162.0, 161.9, 160.0, 156.6, 135.5, 128.5, 120.9, 115.5, 86.1, 59.1, 35.2; HRMS calcd. for $C_{10}H_6N_2O$ [M^+ - ($C_4H_6N_4O$)] 170.0480, found 170.0483.

2,7-Diamino-5-(3-ethoxy-4-hydroxyphenyl)-4-oxo-3,4,5,8-tetrahydropyrido[2,3-*d*]pyrimidine-6-carbonitrile (6o**):**

Isolated as beige solid, (303 mg, 89%), R_f: 0.33, Melting point: 205 – 207 °C; FT-IR: υ (cm^{-1}) = 3500, 3472, 3361, 3161, 2975, 2195, 1673, 1646, 1627, 1560, 1468, 1377, 1286, 1119, 1032; ^{1}H NMR: δ 8.77 (s, 1H), 6.82 (br. s, 3H), 6.69 (d, *J* = 8.1, 1H), 6.52 (dd, *J* = 8.1, 2.0, 1H), 6.05 (br. s, 4H), 4.26 (s, 1H), 4.05 – 3.88 (m, 2H), 1.31 (t, *J* = 7.0, 3H); ^{13}C NMR: δ 163.2, 161.9 (2c), 159.9, 146.7, 146.1, 136.1, 120.9, 119.7, 116.1, 113.6, 86.0, 64.4, 59.0, 35.6, 15.2; HRMS calcd. for $C_{12}H_{10}N_2O_2$ [M^+ - ($C_4H_6N_4O$)] 214.0742, found 214.0747.

2,7-Diamino-4-oxo-5-(thien-2-yl)-3,4,5,8-tetrahydropyrido[2,3-*d*]pyrimidine-6-carbonitrile (6p**):**

Isolated as papaya whip solid, (246 mg, 86%), R_f: 0.12, Melting point: 213 – 215 °C; FT-IR: υ (cm^{-1}) = 3486, 3376, 3152, 2193, 1669, 1622, 1556, 1451, 1398, 1126, 793, 728; ^{1}H NMR: δ 7.33 (dd, *J* = 5.1, 1.1, 1H), 7.07 – 6.95 (m, 3H), 6.93 – 6.88 (m, 1H), 6.35 (br. s, 2H), 6.12 (br. s, 2H), 4.82 (s, 1H); ^{13}C NMR: δ 163.1, 162.1, 161.6, 160.5, 150.6, 127.0, 125.0, 124.7, 120.7, 86.0, 58.5, 31.4; HRMS calcd. for $C_8H_4N_2S$ [M^+ - ($C_4H_6N_4O$)] 160.0095, found 160.0097.

Acknowledgements

We thank Bu-Ali Sina University, Iran National Science Foundation (INSF) (Grant of Allameh Tabataba'i's Award, Grant Number BN093), National Elites Foundation, University of Alicante

(VIGROB-173, UAUSTI16-03), and the Spanish Ministerio de Economía y Competitividad (CTQ2015-66624-P) for financial support to our research groups.

References

1. Anastas, P. T.; Zimmerman, J. B. *Green Chem.* **2016**, *18*, 4324.
2. (a) MohammadiZiarani, G.; Lashgari, N. and Badiei, A. *J. Mol. Catal. A: Chem.* **2016**, *397*, 166; (b) Kaur, M.; Sharma, S. and Bedi, P. M. S. *Chin. J. Catal.* **2015**, *36*, 520; (c) Su, F. and Guo Y. *Green Chem.* **2014**, *16*, 2943; (d) Sani,Y. M.; Daud, W. M. A. W. and Abdul Aziz, A. R. *Appl. Catal. A: Gen.* **2014**, *470*, 140; (e) Gupta, P. and Paul, S. *Catal. Today* **2014**, *236*, 153; (f) Heravi, M. M. and Faghihi, Z. *J. Iran. Chem. Soc.* **2014**, *11*, 209; (g) Firouzabadi, H. and Jafari, A. A. *J. Iran. Chem. Soc.* **2005**, *2*, 85; (h) Firouzabadi, H.; Iranpoor, N. and Khoshnood, A. *Cat. Commun.* **2008**, *9*, 529; (i) Busca, G. *Chem. Rev.* **2007**, *107*, 5366; (j) Okuhara, T. *Chem. Rev.* **2002**, *102*, 3641.
3. Triggle, D. *J. Cell Mol. Neurobiol.* **2003**, *23*, 293.
4. Hilgeroth, A. *Mini Rev. Med. Chem.* **2002**, *2*, 235.
5. (a) Mason, R. P.; Mak, I. T.; Trumbore, M.W.; Mason, P. E. *Am. J. Cardiol.* **1999**, *84*, 16; (b) Aruoma, O.; Smith, C.; Cecchini, R.; Evans, P.; Halliwell, B. Biochem Pharmacol **1991**, *42*, 735.
6. Safak, C.; Simsek, R. *Mini Rev Med Chem.* **2006**, *6*, 747.
7. Kawase, M.; Shah, A.; Gaveriya, H.; Motohashi, N.; Sakagami, H.; Varga, A.; Molnar, J. *Bioorg Med Chem.* **2002**, *10*, 1051.
8. (a) Wan, J-P.; Liu, Y. *RSC Advances* **2012**, *2*, 9763; (b) Comins, D. L.; Higuchi, K.; Young, D. W. *Adv. Heterocyclic Chem.* **2013**, *110*, 175.
9. Hamasaka, G.; Tsuji, H.; Uozumi, Y. *Synlett* **2015**, *26*, 2037.

10. He, T.; Shi, R.; Gong, Y.; Jiang, G.; Liu, M.; Qian, S.; Wang, Z. *Synlett* **2016**, *27*, 1864.

11. Zolfigol, M. A.; Ghorbani Choghamarani, A.; Shahamirian, M.; Safaiee, M.; Mohammadpoor-Baltork, I.; Mallakpour, S. and Abdollahi-Alibeik, M. *Tetrahedron Lett*. **2005**, *46*, 5581.

12. Du, B.X.; Li, Y.L; Wang, X.S.; Shi, D. Q. *J. Heterocyclic Chem.* **2013**, *50*, 534.

13. Niknam, K.; Saberi, D.; NouriSefat, M. *Tetrahedron Lett.* **2009**, *50*, 4058.

14. Niknam, K.; Saberi, D.; Mohagheghnejad, M. *Molecules* **2009**, *14*, 1915.

15. Niknam, K.; Saberi, D.; Sadegheyan, M.; Deris, A. *Tetrahedron Lett*. **2010**, *51*, 692.

16. Niknam, K.; Saberi, D.; NouriSefat, M. *Tetrahedron Lett.* **2010**, *51*, 2959.

17. Niknam, K.; Panahi, F.; Saberi, D.; Mohagheghnejad, M. *J. Heterocyclic Chem.* **2010**, *47*, 292.

18. Niknam, K.; Saberi, D.; Baghernejad, M. *Phosphorus, Sulfur, and Silicon* **2010**, *185*, 875.

19. Niknam, K.; Saberi, D.; Molaee, H.; Zolfigol, M. A. *Can. J. Chem.* **2010**, *88*, 164.

20. Niknam, K.; Mohammadizadeh, M. R.; Mirzaee, S.; Saberi, D. *Chin. J. Chem.* **2010**, *28*, 663.

21. Niknam, K.; Mohammadizadeh, M. R.; Mirzaee, S. *Chin. J. Chem.* **2011**, *29*, 1417.

22. Ghaem, A. A.; Sayed, M.; Baghernejad, M.; Niknam, K. *Chin. J. Chem.* **2012**, *30*, 517.

23. Kiafar, M.; Zolfigol, M. A.; Yarie, M.; Taherpour, A. (A.) *RSC Adv.* **2016**, *6*, 102280.

24. (a) Zolfigol, M. A.; Khakyzadeh, V.; Moosavi-Zare, A. R.; Rostami, A.; Zare, A.; Iranpoor, N. and Beyzavi, M. H.; Luque, R. *Green Chem.* **2013**, *15*, 2132; (b) Yarie, M.; Zolfigol, M. A.; Bayat, Y.; Asgari, A.; Alonso, D. A. and Khoshnood, A. *RSC Adv.*, **2016**, *6*, 82842; (c) Gholinejad, M.; Neshat, A.; Zareh, Fatemeh.; Nájera, C.; Razeghi, M. and Khoshnood, A. *Applied Catalysis A: General*, **2016**, *525*, 31.

25. (a) Liang, X.; Hart, C.; Pang, Q.; Garsuch, A.: Weiss, T.; Nazar, L. F. *Nature Commun.* **2015**, *6*, 5682; (b) Kim, W.; Edri, E.; Frei, Heinz *Acc. Chem. Res.* **2016**, *49*, 1634−1645.